Photoionization cross section of image potential states around nanotubes

2013 Phys. Scr. 87 065602

(http://iopscience.iop.org/1402-4896/87/6/065602)

Phys. Scr. **87** (2013) 065602 (6pp) doi:10.1088/0031-8949/87/06/065602

Photoionization cross section of image potential states around nanotubes

G A Bocan[1,2], S Segui[1,2], J L Gervasoni[1,2,3] and N R Arista[1,3]

[1] Centro Atómico Bariloche, Comisión Nacional de Energía Atómica, Av. Bustillo 9500, 8400 San Carlos de Bariloche, Argentina
[2] Consejo Nacional de Investigaciones Científicas y Técnicas, Argentina
[3] Instituto Balseiro (Universidad Nacional de Cuyo and Comisión Nacional de Energía Atómica), Av. Bustillo 9500, 8400 San Carlos de Bariloche, Argentina

E-mail: segui@cab.cnea.gov.ar

Received 28 May 2012
Accepted for publication 10 April 2013
Published 8 May 2013
Online at stacks.iop.org/PhysScr/87/065602

Abstract
In this paper, we theoretically address the photoemission from image potential states (IPS) around nanotubes. The relevance of this process is related to the fact that this particular kind of IPS has been experimentally detected for carbon nanotubes by means of femtosecond-resolved two-photon photoemission (Zamkov *et al* 2004 *Phys. Rev. Lett.* **93** 156803). The quantum interaction between the bound electron and the incident radiation field is considered within the dipolar approximation, and the transition matrix for the process is obtained using a first-order Born expansion. For a linearly polarized photon with the polarization vector perpendicular to the nanotube's axis, electrons are found to be emitted with a polar angle that is determined by the initial parallel momentum of the bound electron.

PACS numbers: 61.46.Fg, 33.80.Eh

(Some figures may appear in colour only in the online journal)

1. Introduction

Image potential states (or IPS) have concentrated interest in the scientific community in recent years due not only to the variety of systems in which they occur [1–12], but also to the ability of these states to probe the properties of the hosting system at the nanometric scale [13–23]. IPS form in front of surfaces locally polarized by the presence of an external electron: the competition between the Coulomb-like attractive image force experienced by the charge and the repulsive surface results in a potential well where weakly bound electrons can accommodate on a quantized series of states below the vacuum level.

Although IPS were first observed in liquid He by conductivity techniques [24, 25], it was metallic surfaces that provided the most favourable setting for their early study. The successful multiple reflection model of Echenique and Pendry [26] was followed by extensive theoretical work [27] while the development of k-resolved inverse photoemission spectroscopy and two-photon photoemission spectroscopy (2PPES) allowed for the first conclusive experimental evidence of IPS in these systems [1, 28]. The state of the art is the combination of 2PPE with ultrafast laser pulses, a femtosecond resolution technique that has made direct measurements of IPS lifetimes possible [13, 16, 29–31].

A particular kind of IPS has been predicted to form around freely suspended linear molecular conductors or dielectrics, e.g. carbon nanotubes, by Granger *et al* [32]. The centrifugal barrier resulting from their non-zero quantized angular momentum prevents the excited electrons from collapsing into the surface of the tube, thereby substantially increasing their lifetimes at low temperatures, when compared with the ones in planar systems. Experimental evidence of their existence around multiwalled carbon nanotubes (MWNTs) was recently provided by Zamkov *et al* [9], who measured their binding energies and followed their dynamics by means of femtosecond time-resolved photoemission. The use of MWNTs instead of single-walled ones (SWNTs) is due to the tendency of the latter to form bundles [33]. MWNTs constitute an experimentally viable alternative, yielding large quantities of isolated tubes. The observation of IPS in suspended SWNT networks seems to be the future perspective [34].

In this paper, we obtain the cross sections for the emission of photoelectrons occupying an IPS around an isolated, metallic nanotube. Note that the potential on the vacuum

side of an MWNT will have the same analytic form as that of an SWNT and, therefore, theoretical predictions on SWNTs could be contrasted to MWNTs experimental data. We consider the case in which the incident photon is linearly polarized, with its wave vector running perpendicular to the nanotube's axis. In this scenario, the relevant interaction for the process is that between the photon and the bound electron, while we regard the photon–nanotube interaction as playing only a minor role and do not take it into account. We make use of the first-order Born approximation, the dipole approximation and the orthogonalized plane wave approach to obtain the transition matrix corresponding to the photoemission from an IPS. Our results show that when the polarization vector is perpendicular to the nanotube's axis, photoelectrons are emitted in a polar direction that is determined by the parallel momentum of the bound electron. The complementary case of the polarization vector parallel to the axis yields null photoemission.

The paper is organized as follows. In section 2, a theoretical description of the ionization process is presented. In section 3, results for the cross sections are portrayed and discussed. In section 4, the main conclusions reached in this work are summarized. Unless otherwise stated, atomic units are used throughout this paper.

2. Theory

In this work, we follow a procedure analogous to the one presented in a previous paper [35], where the ionization of image electrons by incident free electrons was addressed. The radial wave functions are obtained by numerically solving the Schrödinger equation with an effective potential obtained as the sum of the image potential induced by the bound electron, and the centrifugal potential term [32, 36].

The process to be considered now is that in which an electron occupying an image state around a nanotube is ionized as a result of its interaction with an incident radiation field. The differential probability per unit time for this process to occur is, according to the Fermi Golden Rule,

$$(P_t)_{\mathrm{i}\to\mathrm{f}} = \frac{2\pi}{\hbar}\,|T_{\mathrm{if}}|^2\,\delta\left(E_{\mathrm{f}} - E_{\mathrm{i}} - \hbar\omega_0\right), \tag{1}$$

where E_{i} and E_{f} are the electron's initial and final energy, $\omega_0 = c\,k_0$ is the energy of the incident photon and T_{if} is the transition matrix element which, within a first-order Born approximation, reads

$$T_{\mathrm{if}} = \langle F|\,H_{\mathrm{int}}\,|I\rangle\,. \tag{2}$$

The initial and final states for the system are

$$\begin{aligned} |I\rangle &= \left|1_{\bar{k}_0,\alpha}\right\rangle\,|\Psi_{\mathrm{i}}\rangle\,, \\ |F\rangle &= |0\rangle\,|\Psi_{\mathrm{f}}\rangle\,, \end{aligned} \tag{3}$$

where the first and second ket factors on the right represent the photon (initially one photon with wave vector $\bar{k}_0$ and polarization state α) and electron state, respectively.

The photon–bound electron interaction potential is

$$H_{\mathrm{int}} = -\frac{e}{mc}\,\bar{p}\cdot\bar{A}, \tag{4}$$

where $\bar{p}$ is the momentum operator, and the electromagnetic field operator $\bar{A}$ is given by

$$\bar{A}\,(\bar{r}) = \frac{c}{\sqrt{V}}\sum_{\bar{k},\epsilon_{\mathrm{i}}}\sqrt{\frac{2\pi\hbar}{\omega_{\bar{k}}}}\left(a_{\bar{k},\epsilon_{\mathrm{i}}}\,\mathrm{e}^{\mathrm{i}\bar{k}.\bar{r}} + a^{\dagger}_{\bar{k},\epsilon_{\mathrm{i}}}\,\mathrm{e}^{-\mathrm{i}\,\bar{k}.\bar{r}}\right)\hat{\epsilon}_{\mathrm{i}}, \tag{5}$$

with V the normalization volume and $\hat{\epsilon}_{\mathrm{i}}$ the polarization vector, which is assumed to be linear.

Substituting equations (5), (4) and (3) into equation (2), we obtain the following expression for the transition matrix:

$$T_{\mathrm{if}} = \frac{\mathrm{i}\,\mathrm{e}\,\hbar}{m}\sqrt{\frac{4\pi\hbar}{2\omega_0}}\frac{1}{\sqrt{V}}\,\chi_{\mathrm{if}}, \tag{6}$$

where

$$\chi_{\mathrm{if}} \equiv \langle\Psi_{\mathrm{f}}|\,\mathrm{e}^{\mathrm{i}\frac{\omega_0}{c}\hat{k}_0\bar{r}}\hat{\epsilon}_0\bar{\nabla}\,|\Psi_{\mathrm{i}}\rangle\,. \tag{7}$$

The cross section for a given transition is related to equation (1) via

$$\sigma\left(\bar{k}_0,\hat{\epsilon}_0\right)_{\mathrm{i}\to f} = \frac{(P_t)_{\mathrm{i}\to f}}{j_{\mathrm{photon}}} \tag{8}$$

with $j_{\mathrm{photon}} = c\,n_{\bar{k}_0,\hat{\epsilon}_0}/V$ the incident photon flux and $n_{\bar{k}_0,\hat{\epsilon}_0}$ the number of incident photons in state $(\bar{k}_0,\hat{\epsilon}_0)$. In our case, $n_{\bar{k}_0,\hat{\epsilon}_0} = 1$. Substituting equations (1) and (6) into equation (8), we obtain the total cross section for a given initial state,

$$\begin{aligned} \sigma(\bar{k}_0,\hat{\epsilon}_0) &= \sum_{\bar{k}_{\mathrm{f}}}\frac{(2\pi)^3}{c}\frac{e^2\hbar^2}{m^2\omega_0 2\pi}\delta\left(E_{\mathrm{f}} - E_{\mathrm{i}} - \hbar\omega_0\right)|\chi_{\mathrm{if}}|^2 \\ &= V\int\frac{e^2\hbar^2}{c\,m^2\omega_0 2\pi}\delta\left(E_{\mathrm{f}} - E_{\mathrm{i}} - \hbar\omega_0\right)|\chi_{\mathrm{if}}|^2\,\mathrm{d}\bar{k}_{\mathrm{f}}, \end{aligned} \tag{9}$$

as well as the differential cross section, which reads [37]

$$\frac{\mathrm{d}\sigma\left(\bar{k}_0,\hat{\epsilon}_0\right)}{\mathrm{d}\Omega_{\mathrm{f}}} = V\,\frac{1}{2\pi}\,\frac{e^2}{mc}\,\frac{k_{\mathrm{f}}}{\omega_0}\,|\chi_{\mathrm{if}}|^2\,. \tag{10}$$

We set $\hat{z}$ parallel to the nanotube's axis and the incident photon's wave vector, $\hat{k}_0 = \hat{x}$, perpendicular to it, as is shown in figure 1.

The bound electron is fully delocalized in $\hat{z}$. Its initial state is

$$\begin{aligned} \Psi_{n,l,k_{iz}} &= f_{nl}(\rho)\,\mathrm{e}^{\mathrm{i}\,l\,\varphi}\,\phi_{k_{iz}}(z) \\ &= \frac{\psi_{n,l}(\rho)}{\sqrt{2\pi\rho}}\,\mathrm{e}^{\mathrm{i}\,l\,\varphi}\,\frac{\mathrm{e}^{\mathrm{i}\,k_{iz}\,z}}{\sqrt{L}}, \end{aligned} \tag{11}$$

with L a normalization length in $\hat{z}$.

The tubular image potential, although long-range in character ($V_{\mathrm{im}} \approx 1/(\rho\log\rho)$ [32]), presents a slightly milder behaviour than the Coulomb potential. As shown by previous work [38], a first-order Born treatment of the transition matrix elements based on plane waves for the continuum states provides a correct description of the scattering amplitude even

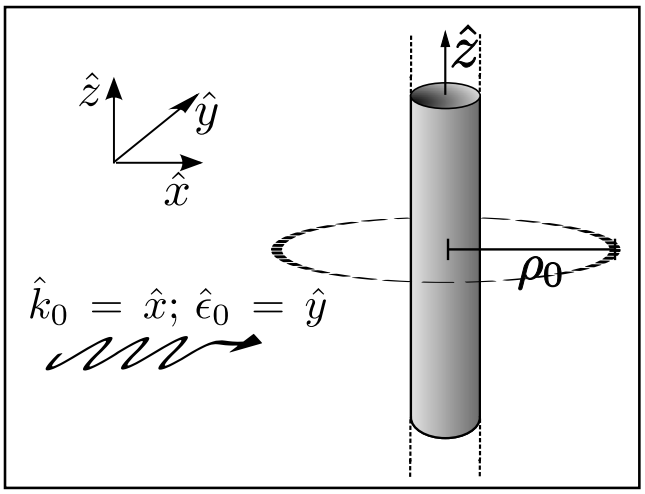

Figure 1. System's geometry. The bound electron is delocalized in the $\hat{z}$-direction. ρ_0 is a characteristic electron–nanotube distance. The incident photon wave vector is $\bar{k}_0 = k_0\,\hat{x}$ and its polarization state $\hat{\epsilon}_0$ is perpendicular to the nanotube's axis.

for a pure Coulombic potential. Therefore, we assume that it also applies as a first-order approximation to our system. Our ionized state is then a plane wave, orthogonalized with respect to the initial bound state as in [35],

$$|\mathrm{OPW_f}\rangle = |\mathrm{PW_f}\rangle - |\Psi_\mathrm{i}\rangle\,\langle\Psi_\mathrm{i}\,|\mathrm{PW_f}\rangle\,. \tag{12}$$

The last bracket can be readily evaluated as follows:

$$\begin{aligned}\langle \mathrm{PW_f}\,|\Psi_\mathrm{i}\rangle &= \int \frac{\mathrm{e}^{-\mathrm{i}\bar{k}_\mathrm{f}.\bar{r}}}{\sqrt{V}}\,\frac{\psi_{n,l}\,(\rho)}{\sqrt{2\pi\rho}}\,\mathrm{e}^{\mathrm{i}l\varphi}\,\frac{\mathrm{e}^{\mathrm{i}k_{iz}z}}{\sqrt{L}}\mathrm{d}\bar{r}\\ &= \delta_{k_{\mathrm{f}z},k_{iz}}\frac{2\pi}{\sqrt{A}}\,\mathrm{e}^{\mathrm{i}l\,(\varphi_\mathrm{f}-\pi/2)}I_1\left(k_{\mathrm{f}\|}\right),\end{aligned} \tag{13}$$

where $A = V/L$ and we have used the Jacobi–Anger identity [39] to integrate over φ. The integral in ρ is

$$I_1\left(k_{\mathrm{f}\|}\right) \equiv \int \frac{\psi_{n,l}\,(\rho)}{\sqrt{2\pi\rho}}\,\rho\,J_l\left(k_{\mathrm{f}\|}\rho\right)\,\mathrm{d}\rho, \tag{14}$$

with $J_l(k_{\mathrm{f}\|}\,\rho)$ the Bessel function of order l and $\bar{k}_{\mathrm{f}\|}$ the projection of $\bar{k}_\mathrm{f}$ to the xy-plane.

Finally, note that [32, 35]

$$\begin{aligned}\rho_0 &\sim 10^2\ \mathrm{au},\\ \left|E_{n,l}\right| &\sim 10^{-4}\ \mathrm{au},\end{aligned} \tag{15}$$

where ρ_0 is a characteristic electron–nanotube distance. The energies ω_0 of interest are

$$\omega_0 \sim \left|E_{n,l}\right| \ll 1, \tag{16}$$

and so we are entitled, in equation (7), to consider the dipole approximation ($c = 137$ au)

$$\begin{aligned}\frac{\omega_0}{c}\,\hat{k}_0\cdot\bar{r} \propto \frac{\omega_0}{c}\rho_0 \ll 1,\\ \mathrm{e}^{\mathrm{i}\frac{\omega_0}{c}\hat{k}_0\cdot\bar{r}} \approx 1.\end{aligned} \tag{17}$$

Combined with the OPW approximation (equation (12)), this leads to

$$\begin{aligned}\chi_\mathrm{if}^\mathrm{OPW} &= \langle \mathrm{OPW_f}|\,\hat{\epsilon}_0.\bar{\nabla}\,|\Psi_\mathrm{i}\rangle\\ &= \langle \mathrm{PW_f}|\,\hat{\epsilon}_0.\bar{\nabla}\,|\Psi_\mathrm{i}\rangle - \langle \mathrm{PW_f}\,|\Psi_\mathrm{i}\rangle\,\langle\Psi_\mathrm{i}|\,\hat{\epsilon}_0.\bar{\nabla}\,|\Psi_\mathrm{i}\rangle\\ &= \chi_\mathrm{if}^{PW} - \langle PW_\mathrm{f}\,|\Psi_\mathrm{i}\rangle\,\langle\Psi_\mathrm{i}|\,\hat{\epsilon}_0.\bar{\nabla}\,|\Psi_\mathrm{i}\rangle\,.\end{aligned} \tag{18}$$

The expression obtained for the matrix element (equation (18)) is valid for any fixed polarization vector $\hat{\epsilon}_0$. For the case considered ($\bar{k}_0 \parallel \hat{x}$, as shown in figure 1), there are two independent directions for $\hat{\epsilon}_0$, namely parallel to the nanotube's axis ($\hat{\epsilon}_0 = \hat{z}$), or perpendicular to it ($\hat{\epsilon}_0 = \hat{y}$). The former case does not contribute to the photoionization process: no electrons are to be emitted when the incident electric field points in the $\hat{z}$-direction, along which image electrons can move freely.

When the polarization is perpendicular to the tube's axis, the matrix element (18) can be evaluated in a straightforward way (see appendix A). In this case, the orthogonalization term is identically zero and we obtain

$$\begin{aligned}\chi_\mathrm{if}^\mathrm{OPW} &= \chi_\mathrm{if}^\mathrm{PW}\\ &= \mathrm{i}\,\delta_{k_{iz},k_{\mathrm{f}z}}\,\frac{2\pi}{\sqrt{A}}\,\mathrm{e}^{\mathrm{i}\,l\,(\varphi_\mathrm{f}-\pi/2)}\,\sin\varphi_\mathrm{f}\,R_1\left(k_{\mathrm{f}\|}\right)\end{aligned} \tag{19}$$

with

$$R_1\left(k_{\mathrm{f}\|}\right) \equiv \int\left[l\,f_{nl}\,(\rho) - \rho\,\frac{\partial f_{nl}\,(\rho)}{\partial\rho}\right]J_{(l+1)}\left(k_{\mathrm{f}\|}\,\rho\right)\,\mathrm{d}\rho. \tag{20}$$

Regarding this result note that: (i) it does not depend on the function chosen to model $\psi_{n,l}(\rho)$; (ii) if we do not consider the dipole approximation, we obtain $\chi_\mathrm{if}^\mathrm{OPW} \approx \chi_\mathrm{if}^\mathrm{PW}$; and (iii) there is a marked contrast between the negligible OPW correction obtained here, with the central role it played in our previous work on ionization by electron impact [35].

3. Results

In order to obtain the differential cross section, we substitute equation (19) into equation (10) and obtain

$$\frac{\mathrm{d}\sigma}{\mathrm{d}\Omega_\mathrm{f}} = (2\pi)^3\,\frac{e^2\,k_\mathrm{f}}{2\pi\,mc\omega_0}\,\delta\left(k_{\mathrm{f}z} - k_{iz}\right)\left|R_1\left(k_{\mathrm{f}\|}\right)\right|^2\sin^2\varphi_\mathrm{f}, \tag{21}$$

where we find a simple $\sin^2\varphi_\mathrm{f}$ dependence for the azimuthal angle and a fully localized distribution ($\cos\theta_\mathrm{f} = k_{\mathrm{i}z}/k_\mathrm{f}$) in the polar angle θ_f. The total cross section reads

$$\sigma = (2\pi)^3\,\frac{e^2}{mc\,\omega_0\,2}\left|R_1\left(\sqrt{2\left(E_{n,l}+\omega_0\right)}\right)\right|^2, \tag{22}$$

where we have used the energy conservation equation $E_{n,l} + k_{iz}^2/2 + \omega_0 = k_\mathrm{f}^2/2$. In figure 2, σ is plotted as a function of the incident radiation energy ω_0 for initial electronic states $\{n = 1, l\}$, with $l = 5, \ldots, 8$; the corresponding binding energies are given in table 1, along with the position ρ_0 at which the squared radial wave function presents its maximum values for a nanotube of radius 0.68 nm.

Table 1. Binding energies and maximum probability radius ρ_0 for the first four bound image potential states for a nanotube of 0.68 nm radius.

l	$E_{1,l}$ (meV)	ρ_0 (nm)
5	−14.005	6.66
6	−7.651	10.16
7	−4.845	15.50
8	−3.294	21.89

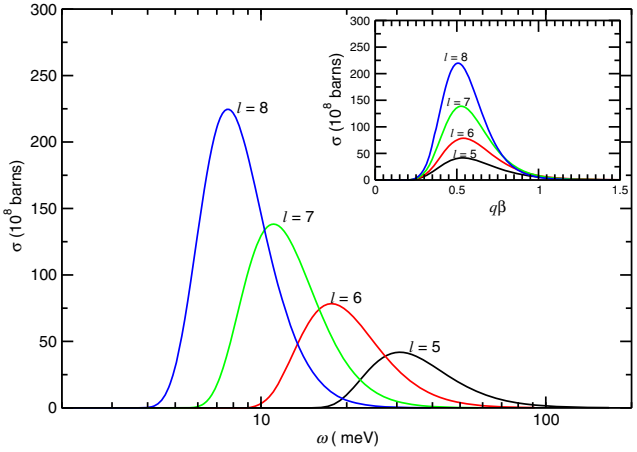

Figure 2. Total ionization cross sections for initial electronic states $\{n, l\}$ with $n = 1$ and $l = 5, \ldots, 8$. The incident photon is polarized perpendicular to the nanotube's axis. The interaction is treated within the dipole approximation. The OPW is used to represent the ionized state. In the inset, the cross section is plotted as a function of the variable $q\beta$, as suggested from equation (24).

In addition to the usual ionization threshold at $\omega_0 = |E_{n,l}|$, the curves present a peaked maximum at $\omega_0 \approx 2|E_{n,l}|$. The amplitudes of these peaks decay with a power law as a function of the absolute value of the binding energy, with an exponent of ≈ 1.2 (i.e. $\sigma_{\max} \propto E_{n,l}^{-1.2}$). In comparison with the photoionization of the hydrogen atom, for which cross section values are of the order of 1 Mb for the 1s state near the ionization threshold, we observe that the probability of extracting an electron from an image-potential state is at least 10^3 times larger.

In order to discuss the marked features of the calculated cross sections, we use an analytical form to describe the radial part of the wave function,

$$\psi_{n,l} \approx \sqrt{\frac{\rho^{\alpha-1}\,\mathrm{e}^{-\rho/\beta}}{\beta^{\alpha}\Gamma(\alpha)}}, \tag{23}$$

where $\Gamma(x)$ is the usual Gamma function; for each set $\{n, l\}$, the parameters α and β are chosen so that it reproduces the numerical eigenfunctions [35, 36]. We substitute this expression into the radial integral R_1 in equation (20) and obtain

$$\begin{aligned} R_1(q) &\approx \int \sqrt{\frac{\rho^{\alpha-1}\,\mathrm{e}^{-\rho/\beta}}{\beta^{\alpha}\Gamma(\alpha)}}\,\frac{1}{\sqrt{2\pi\rho}}\left(-\frac{\alpha}{2}+\frac{\rho}{2\beta}+l+1\right) \\ &\quad\times J_{l+1}(q\,\rho)\,\mathrm{d}\rho \\ &\approx \frac{1}{\sqrt{2\pi}\;(q\beta)^{\alpha}\,\Gamma(\alpha)}\int_0^{+\infty}\mathrm{e}^{-t/(2q\beta)}\,t^{\alpha/2}\,J_l(t)\,\mathrm{d}t, \end{aligned} \tag{24}$$

where we have made the substitution $t = \rho\, q$, and applied some well-known properties of Bessel functions and of integrals involving them [39].

It is clear from equation (24) that the radial integral R_1 can be expressed as $R_{1\alpha}(q\beta)$, that is, it is a function of $q\beta$ with α being a parameter. The variable $q\beta$ is dimensionless with $q = \sqrt{2(E_{n,l} + \omega_0)}$ and β playing the role of a characteristic distance. Furthermore, it could be shown that the ionization cross section is itself a function of $q\beta$, and we can see in the inset of figure 2 that its maximum occurs when $q\beta \approx 0.5$. This result is analogous to what one finds, for example, in the photoionization of the hydrogen atom when using a plane wave for the ejected electron [37].

The present cross section calculations allow us to give an estimate for the mean lifetime of an IPS due to its interaction with ambient (solar) radiation. Considering the flux of solar radiation reaching the terrestrial surface [40], we obtain a lifetime of $\tau = 0.7$ s for the state $n = 1$, $l = 7$ and a photon energy of 10 meV (for which $\sigma_{1,7}$ is maximum). This is considerably larger than the lifetime obtained from other decay mechanisms cited by Granger *et al*, such as the collapse of image state electrons into the bulk due to tunnelling through the centrifugal barrier.

Finally, it is important to recall that photoionization is the basis of 2PPE spectroscopy, the main technique used in the detection of IPS. Although quantitative comparisons would be difficult to accomplish, our calculations could be applied in a qualitative analysis of measured spectra, e.g. for determining the relative height of the detected peaks corresponding to different IPSs. The procedure described here is general and can be applied using different forms of the bound wave functions such as the low angular momentum states detected by Zamkov *et al* [9].

4. Summary

This paper presents a quantum theoretical description of the emission of photoelectrons occupying image potential states, with thorough calculations of differential and total cross sections. The study yields a series of predictions that may be subject to experimental tests. First, the process presents a null cross section if the incident radiation is polarized parallel to the nanotube's axis. For the perpendicular case, emission occurs at a polar angle that is determined by the initial parallel momentum of the bound electron. The ionization cross section presents a peaked maximum, reaching very high values for photon energies of the order of the ionization threshold, and going rapidly to zero afterwards.

The OPW term introduces no sensitive change to the plane wave result. This is in contrast with our previous work on ionization of image electrons by electron impact, where this correction was central for obtaining the correct behaviour of the cross section for high impact energies.

Given the general character of the present formulation, we expect this work to be useful in relation to current experimental efforts to detect and characterize the properties of these states, and to provide new insights regarding image electron emission from cylindrical nanostructures.

Acknowledgments

We are grateful to Dr J E Miraglia and R A Barrachina for fruitful discussions. This work was supported in part by Universidad Nacional de Cuyo and CONICET from Argentina.

Appendix A. Matrix elements

In equation (18), we take $\hat{\epsilon}_0 = \hat{y}$ and evaluate separately the PW and the correction contributions. We begin with the plane wave term

$$\begin{aligned}\chi_{\rm if}^{\rm PW} &= \int \frac{{\rm e}^{-{\rm i}\bar{k}_{\rm f}.\bar{r}}}{\sqrt{V}} \frac{\partial}{\partial y}\Psi_{\rm i}\left(\bar{r}\right) {\rm d}\bar{r} \\ &= \int \frac{{\rm e}^{-{\rm i}\bar{k}_{\rm f}.\bar{r}}}{\sqrt{V}} {\rm e}^{{\rm i}\,l\,\varphi}\phi_{k_{iz}}\left(z\right) \\ &\quad \times \left[\sin\varphi \frac{\partial f_{nl}\left(\rho\right)}{\partial\rho} + \frac{\cos\varphi}{\rho}\,{\rm i}\,l\,f_{nl}\left(\rho\right)\right] {\rm d}\bar{r}.\end{aligned} \tag{A.1}$$

We integrate over z, make use of the Jacobi–Anger identity to integrate over φ, do some more algebra and obtain

$$\begin{aligned}\chi_{\rm if}^{\rm PW} &= (-1)\,\delta_{k_{\rm fz},k_{iz}} \frac{2\pi}{\sqrt{A}} \frac{1}{2}\,{\rm e}^{{\rm i}\,l\,(\varphi_{\rm f}-\pi/2)} \\ &\quad \times \left\{{\rm e}^{-{\rm i}\,\varphi_{\rm f}}\,R_2\left(k_{\rm f\|}\right) - {\rm e}^{{\rm i}\,\varphi_{\rm f}}\,R_1\left(k_{\rm f\|}\right)\right\}\end{aligned} \tag{A.2}$$

with

$$\begin{aligned}R_1(q) &\equiv \int \left[l\,f_{nl}\left(\rho\right) - \rho\,\frac{\partial f_{nl}\left(\rho\right)}{\partial\rho}\right] J_{(l+1)}\left(q\rho\right)\,{\rm d}\rho, \\ R_2(q) &\equiv \int \left[l\,f_{nl}\left(\rho\right) + \rho\,\frac{\partial f_{nl}\left(\rho\right)}{\partial\rho}\right] J_{(l-1)}\left(q\rho\right)\,{\rm d}\rho.\end{aligned} \tag{A.3}$$

Finally, we make use of the result $R_1(q) = R_2(q)$ (see appendix B) and obtain

$$\chi_{\rm if}^{\rm PW} = {\rm i}\,\delta_{k_{iz},k_{\rm fz}} \frac{2\pi}{\sqrt{A}}\,{\rm e}^{{\rm i}\,l\,(\varphi_{\rm f}-\pi/2)}\,\sin\varphi_{\rm f}\,R_1\left(k_{\rm f\|}\right). \tag{A.4}$$

Regarding the second term in the matrix element (18), we note that

$$\begin{aligned}\langle\Psi_{\rm i}|\,\hat{y}.\bar{\nabla}\,|\Psi_{\rm i}\rangle &= \int \Psi_{\rm i}\left(\bar{r}\right) \frac{\partial}{\partial y}\Psi_{\rm i}\left(\bar{r}\right)\,{\rm d}\bar{r} \\ &= \int f_{nl}^{*}\left(\rho\right) \frac{\partial f_{nl}\left(\rho\right)}{\partial\rho}\,\rho\,{\rm d}\rho \int \sin\varphi\,{\rm d}\varphi \\ &\quad + \int f_{nl}^{*}\left(\rho\right) \frac{i\,l}{\rho}\,f_{nl}\left(\rho\right)\,\rho\,{\rm d}\rho \int \cos\varphi\,{\rm d}\varphi \\ &= 0\end{aligned} \tag{A.5}$$

and the orthogonalization correction is therefore null.

Appendix B. R_1 and R_2

In this appendix we will prove the identity $R_1 = R_2$, used in equation (A.4). We use the recurrence relation [39]

$$J_{l+1}(q\rho) = \frac{2\,l}{q\rho}\,J_l(q\rho) - J_{l-1}(q\rho) \tag{B.1}$$

to substitute in the definition of R_1 given in equations (A.3),

$$\begin{aligned}R_1(q) &= \int_0^\infty \left\{l\frac{f_{nl}(\rho)}{\rho} - \frac{\partial f_{nl}}{\partial\rho}\right\} \\ &\quad \times \left(\frac{2l}{q\rho}\,J_l(q\rho) - J_{l-1}(q\rho)\right)\,\rho\,{\rm d}\rho \\ &= -\int_0^\infty \left\{l\frac{f_{nl}(\rho)}{\rho} - \frac{\partial f_{nl}}{\partial\rho}\right\}\,J_{l-1}(q\rho)\,\rho\,{\rm d}\rho \\ &\quad + 2l^2\int_0^\infty f_{nl}(\rho)\,\frac{J_l(q\rho)}{q\rho}\,{\rm d}\rho \\ &\quad - 2l\int_0^\infty \frac{\partial f_{nl}}{\partial\rho}\,\frac{J_l(q\rho)}{q\rho}\,\rho\,{\rm d}\rho.\end{aligned} \tag{B.2}$$

The last integral can be solved by parts and, assuming that f_{nl} is a well-behaved function in the limits of integration, we can write

$$\begin{aligned}R_1(q) &= -\int_0^\infty \left\{l\frac{f_{nl}(\rho)}{\rho} - \frac{\partial f_{nl}}{\partial\rho}\right\}\,J_{l-1}(q\rho)\,\rho\,{\rm d}\rho \\ &\quad + 2l^2\int_0^\infty f_{nl}(\rho)\,\frac{J_l(q\rho)}{q\rho}\,{\rm d}\rho \\ &\quad + 2l\int_0^\infty f_{nl}(\rho)\,\frac{\partial J_l(q\rho)}{\partial(q\rho)}\,{\rm d}\rho.\end{aligned} \tag{B.3}$$

Now we use the identity $J_l'(x) = J_{l-1}(x) - \frac{l}{x}J_l(x)$ and obtain

$$\begin{aligned}R_1(q) &= \int_0^\infty \left(\frac{l}{\rho}\,f_{nl}(\rho) + \frac{\partial f_{nl}}{\partial\rho}\right)\,J_{l-1}(q\rho)\,{\rm d}\rho \\ &= R_2(q).\end{aligned} \tag{B.4}$$

References

[1] Dose V, Altmann W, Goldmann A, Kolac U and Rogozik J 1984 Image-potential states observed by inverse photoemission *Phys. Rev. Lett.* **52** 1919–21

[2] Straub D and Himpsel F J 1984 Identification of image-potential surface states on metals *Phys. Rev. Lett.* **52** 1922–4

[3] Goldman J R and Prybyla J A 1994 Ultrafast dynamics of laser-excited electron distributions in silicon *Phys. Rev. Lett.* **72** 1364–7

[4] Lehmann J, Merschdorf M, Thon A, Voll S and Pfeiffer W 1999 Properties and dynamics of the image potential states on graphite investigated by multiphoton photoemission spectroscopy *Phys. Rev.* B **60** 17037–45

[5] Borisov A G, Hakala T, Puska M J, Silkin V M, Zabala N, Chulkov E V and Echenique P M 2007 Image potential states of supported metallic nanoislands *Phys. Rev.* B **76** 121402

[6] Rohleder M, Berthold W, Güdde J and Höfer U 2005 Time-resolved two-photon photoemission of buried interface states in Ar/Cu(100) *Phys. Rev. Lett.* **94** 017401

[7] Yamamoto I, Mikamori M, Yamamoto R, Yamada T, Miyakubo K, Ueno N and Munakata T 2008 Resonant two-photon photoemission study of electronically excited states at the lead phthalocyanine/graphite interface *Phys. Rev.* B **77** 115404

[8] Yang Q, Muntwiler M and Zhu X-Y 2009 Charge transfer excitons and image potential states on organic semiconductor surfaces *Phys. Rev.* B **80** 115214

[9] Zamkov M, Woody N, Shan B, Chakraborty H S, Chang Z, Thumm U and Richard P 2004 Time-resolved photoimaging of image-potential states in carbon nanotubes *Phys. Rev. Lett.* **93** 156803

[10] Feng M, Zhao J and Petek H 2008 Atomlike, hollow-corebound molecular orbitals of C_{60} *Science* **320** 359–62

[11] Zhao J, Feng M, Yang J and Petek H 2009 The superatom states of fullerenes and their hybridization into the nearly free electron bands of fullerites *ACS Nano* **3** 853–64

[12] Armbrust N, Güdde J, Jakob P and Höfer U 2012 Time-resolved two-photon photoemission of unoccupied electronic states of periodically rippled graphene on Ru(0001) *Phys. Rev. Lett.* **108** 056801

[13] Höfer U, Shumay I L, Reuß Ch, Thomann U, Wallauer W and Fauster Th 1997 Time-resolved coherent photoelectron spectroscopy of quantized electronic states on metal surfaces *Science* **277** 1480–2

[14] Hertel T, Knoesel E, Wolf M and Ertl G 1996 Ultrafast electron dynamics at Cu(111): response of an electron gas to optical excitation *Phys. Rev. Lett.* **76** 535–8

[15] Miller A D, Bezel I, Gaffney K J, Garret-Roe S, Liu S H, Szymanski P and Harris C B 2002 Electron solvation in two dimensions *Science* **297** 1163–6

[16] Berthold W, Höfer U, Feulner P, Chulkov E V, Silkin V M and Echenique P M 2002 Momentum-resolved lifetimes of image-potential states on Cu(100) *Phys. Rev. Lett.* **88** 056805

[17] Marinica D C, Ramseyer C, Borisov A G, Teillet-Billy D, Gauyacq J P, Berthold W, Feulner P and Höfer U 2002 Effect of an atomically thin dielectric film on the surface electron dynamics: image-potential states in the Ar/Cu(100) system *Phys. Rev. Lett.* **89** 046802

[18] Padowitz D F, Merry W R, Jordan R E and Harris C B 1992 Two-photon photoemission as a probe of electron interactions with atomically thin dielectric films on metal surfaces *Phys. Rev. Lett.* **69** 3583–6

[19] Lingle R L, Padowitz D F, Jordan R E, McNeill J D and Harris C B 1994 Two-dimensional localization of electrons at interfaces *Phys. Rev. Lett.* **72** 2243–6

[20] Schmitz-Hübsch T, Oster K, Radnik J and Wandelt K 1995 Photoemission from quantum-well states in ultrathin Xe crystals *Phys. Rev. Lett.* **74** 2595–8

[21] Loly P D and Pendry J B 1983 Removing the limits to accurate band-structure determination by photoemission *J. Phys. C: Solid State Phys.* **16** 423–31

[22] Fischer N, Schuppler S, Fischer R, Fauster Th and Steinmann W 1993 Image states and the proper work function for a single layer of Na and K on Cu(111), Co(0001) and Fe(110) *Phys. Rev.* B **47** 4705–13

[23] Memmel N and Bertel E 1995 Role of surface states for the epitaxial growth on metal surfaces *Phys. Rev. Lett.* **75** 485–8

[24] Brown T R and Grimes C C 1972 Observation of cyclotron resonance in surface-bound electrons on liquid helium *Phys. Rev. Lett.* **29** 1233–6

[25] Grimes C C and Brown T R 1974 Direct spectroscopic observation of electrons in image-potential states outside liquid helium *Phys. Rev. Lett.* **32** 280–3

[26] Echenique P M and Pendry J B 1978 The existence and detection of Rydberg states at surfaces *J. Phys. C: Solid State Phys.* **11** 2065

[27] Echenique P M, Berndt R, Chulkov E V, Fauster Th, Goldmann A and Höfer U 2004 Decay of electronic excitations at metal surfaces *Surf. Sci. Rep.* **52** 219–317

[28] Giesen K, Hage F, Himpsel F J, Riess H J and Steinmann W 1985 Two-photon photoemission via image-potential states *Phys. Rev. Lett.* **55** 300–3

[29] Schoenlein R W, Fujimoto J G, Eesley G L and Capehart T W 1988 Femtosecond studies of image-potential dynamics in metals *Phys. Rev. Lett.* **61** 2596–9

[30] Schoenlein R W, Fujimoto J G, Eesley G L and Capehart T W 1990 Femtosecond dynamics of the $n = 2$ image-potential state on Ag(100) *Phys. Rev.* B **41** 5436–9

[31] Shumay I L, Höfer U, Reuß Ch, Thomann U, Wallauer W and Fauster Th 1998 Lifetimes of image-potential states on Cu(100) and Ag(100) measured by femtosecond time-resolved two-photon photoemission *Phys. Rev.* B **58** 13974–81

[32] Granger B E, Král P, Sadeghpour H R and Shapiro M 2002 Highly extended image states around nanotubes *Phys. Rev. Lett.* **89** 135506

[33] Liu J *et al* 1998 Fullerene pipes *Science* **280** 1253–6

[34] Homma Y, Kobayashi Y, Ogino T and Yamashita T 2002 Growth of suspended carbon nanotube networks on 100 nm-scale silicon pillars *Appl. Phys. Lett.* **81** 2261

[35] Bocan G A, Arista N R, Gervasoni J L and Segui S 2008 Ionization from image states around nanotubes *Phys. Rev.* B **77** 035438

[36] Segui S, Celedón López C, Bocan G A, Gervasoni J L and Arista N R 2012 Tubular image states: general formulation and properties for metallic and non-metallic nanotubes *Phys. Rev.* B **85** 235441

[37] Greiner W 1998 *Quantum Mechanics–Special Chapters* (Berlin: Springer)

[38] Macek J H and Barrachina R O 1990 Born expansions for charged particle scattering *Comments At. Mol. Phys.* **24** 287–97

[39] Abramowitz M and Stegun I (ed) 1970 *Handbook of Mathematical Functions* (New York: Dover) chapter 9 pp 355–434

[40] Reif F 1967 Statistical physics *Berkeley Physics Course* vol 5 (New York: McGraw-Hill)